Desalination and Water Treatment
www.deswater.com
doi: 10.5004/dwt.2019.24401

163 (2019) 155–165
September

Synthesis of magnetic rectorite/humic acid/chitosan composite for removal of heavy metal ions from water

Xiao Zhu[a], Yu-bin Tang[a,b,*], Fang-yan Chen[a,*], Yu Shi[a], Xin-gang Wang[a]

[a]*School of Environmental and Chemical Engineering, Jiangsu University of Science and Technology, Zhenjiang Jiangsu, 212003 China, Tel. +86-511-84448601; email: ybbill@163.com (Y.-b. Tang), Tel. +86-511-85605157; emails: catchen1029@sohu.com (F.-y. Chen), zhuxiao_93@163.com (X. Zhu), 291197172@qq.com (Y. Shi), hofs@163.com (X.-g. Wang)*
[b]*Institute of industrial technology, Zhangjiagang Campus of Jiangsu University of Science and Technology, 215600 China*

Received 21 August 2018; Accepted 10 May 2019

ABSTRACT

Rectorite (REC) was modified by using hexadecyl trimethyl ammonium bromide (CTAB) to prepare REC-CTAB. Fe_3O_4 particles were introduced into the interlayer space of the CTAB-modified REC to form Fe_3O_4/REC-CTAB. Then humic acid (HA) and chitosan (CTS) were loaded on the surface of Fe_3O_4/REC-CTAB to prepare magnetic composite HA/CTS/Fe_3O_4/REC-CTAB by sol-gel method. The performance of the composite was characterized by scanning electron microscope, transmission electron microscope, X-ray diffraction, vibrating sample magnetometer and fourier transform infrared spectroscopy. The specific surface area, pore size distribution and pore volume of the composite were determined by N_2-BET method. The composite was used to remove Cu^{2+}, Cd^{2+} and Pb^{2+} from aqueous solutions, the adsorptive isotherms were measured, and the adsorption kinetics and regeneration of the adsorbents were investigated. The results show that the composite prepared is a mesoporous material with high specific surface area, it has strong ability to adsorb the three heavy metal ions, and the saturation adsorption capacity for Cu^{2+}, Cd^{2+} and Pb^{2+} could reach 128.04, 105.15 and 221.24 mg/g, respectively, at 298 K. The isothermal adsorption data for each ion were well fitted to the Freundlich and Langmuir models, and the adsorption kinetics conforms to the pseudo-second-order kinetics equation. The composite material exhibited superparamagnetic behavior with small coercivity in the applied magnetic fields, and could be separated from aqueous solution with an appropriate magnet. Moreover, the magnetic composite used can be regenerated by HCl solution and retained a good adsorption capacity to be reused many times. This work suggests that the magnetic composite has a potential application value in treatment of heavy metal wastewater.

Keywords: Rectorite; Magnetic adsorbent; Heavy metals; Preparation; Characterization

1. Introduction

Nowadays, with the rapid development of modern industry, the wastewater containing heavy metal ions causes severe environmental pollution. Heavy metal ions are toxic at low concentration, non-biodegradable, bioaccumulative and have biological magnification effect [1]. Therefore, it is of great significance to remove heavy metal ions from wastewater for protecting environment and human health. There are many ways to deal with heavy metal ion containing wastewater, such as, ion exchange, chemical precipitation, adsorption, electrodeposition, membrane filtration, electroplating, reverse osmosis, etc., but some of these techniques have drawbacks, for example, disposal of residual metal sludge or high cost. Nevertheless, due to high efficiency, easy handling and cost-effectiveness, adsorption technique

* Corresponding authors.

exhibits many advantages [2,3]. Many studies have shown that clay mineral such as kaolinite, montmorillonite, bentonite and rectorite have good adsorption and ion exchange properties, and can be used to remove heavy metal ions or organic pollutants in wastewater. However, these minerals can fully exert the role of adsorption and ion exchange when used only in powder form, the particle of this kind of powder mineral is very small, and it will remain suspended in water for a long time after treatment of wastewater. That is to say, it is difficult to realize the solid–liquid separation, so the mineral's application in wastewater treatment was limited [4]. The method to solve this problem is to combine magnetic materials with clay minerals or other materials so that the composite with excellent magnetic properties, good adsorption capacity and ion exchange performance could be prepared. After being used to treat wastewater, the composite can be quickly separated from the aqueous phase by using magnetic separation technology, so the adsorbent can be efficiently recovered and reused [1,5,6].

Rectorite is a novel environmental material, which is arousing many researchers' attention. It is an interstratified layered silicate mineral consisting of a regular stacking of dioctahedral mica-like layer and dioctahedral smectite-like layer in a ratio of 1:1, with advantages of high temperature resistance, hydrophilicity, good dispersity in water, good expansibility and so on. There are exchangeable cations in its interlayer, which can react with other metal ions by ion exchange [7,8]. However, the adsorptive performance of rectorite is limited due to the hydrolyzability of the cations existed at interlayer. So rectorite must be modified to broaden its interlayer spacing, and then the adsorption capacity could be enhanced. Wang et al. [9] introduced cetyl trimethylammonium bromide (CTAB) and Fe_3O_4 into the interlayers of raw rectorite. The results suggested that the obtained composite REC/Fe_3O_4-CTAB exhibited better adsorptive performance of nitrate and phosphate when Fe_3O_4 was loaded on REC ahead of CTAB. Hong et al. [10] modified REC by stearyl trimethyl ammonium chloride and effectively increased the adsorption capacity of Cr(VI) in wastewater. Xie et al. [6] provided an idea for preparation of magnetic nanoparticles using organic rectorite as a carrier, chitosan/organic rectorite-Fe_3O_4 composite microspheres was synthesized. The microspheres could be used to remove heavy metals in wastewater with low concentration. The surface of humic acid is negatively charged, and it has the ability to bind metal ions. Clay minerals can remove humic acid in water to some extent, and the two have adsorption capacity for heavy metals [11]. Chitosan molecules contain a lot of amino and hydroxyl groups, which can form stable chelates with most of the transition metal ions. Chitosan has strong ability to remove Cu^{2+}, Pb^{2+}, Cd^{2+}, Zn^{2+}, Ni^{2+} and Ag^{+} in wastewater, thus making it an important alternative adsorbent for heavy metal removal [12–15].

In the present study, rectorite was organo-modified by using hexadecyl trimethyl ammonium bromide (CTAB) to form REC-CTAB, then magnetic rectorite (Fe_3O_4/REC-CTAB) was prepared by in-situ intercalation method (i.e., introducing Fe_3O_4 into the interlayers of REC-CTAB), and then, HA and CTS were loaded on the surface of Fe_3O_4/REC-CTAB through sol-gel method to form composite HA/CTS/Fe_3O_4/REC-CTAB. The aim is to achieve high-efficient removal of heavy metal ions in wastewater and efficient recovery of the adsorbents.

2. Experimental section

2.1. Materials and instruments

Materials employed: ethanol, sodium tripolyphosphate (STPP), cetyl trimethyl ammonium bromide (CTAB), hydrochloric acid, sodium hydroxide, ferric chloride ($FeCl_3{\cdot}6H_2O$), ferrous sulfate ($FeSO_4{\cdot}7H_2O$), ammonia ($NH_3{\cdot}H_2O$), polyvinylpyrrolidone K-30 (PVP), acetic acid, chitosan, cadmium nitrate, lead nitrate, copper nitrate were all of analytical grade and purchased from Sinopharm Chemical Reagent Co. Ltd. (Shanghai, China).

Main Instruments and Equipments: AA-6300 atomic absorption spectrophotometer (Shimadzu Instrument Co. Ltd., Japan); magnetic heating stirrer (79-2 type); DKZ-2 electric constant temperature oscillation flume (Shanghai Precision Laboratory Equipment Co. Ltd., Shanghai, China).

2.2. Preparation of the adsorbents

2.2.1. Purification of rectorite

10 g of REC was added into 100 mL of deionized water to form aqueous suspension with 10% rectorite (w/w), and dispersed by ultrasound for 40 min, settled for 3 h, separated out the supernatant by centrifugalization, then dried at 60°C for 12 h, ground and screened with 200 mesh standard sieve [16].

2.2.2. Organo-modification of rectorite

4 g of rectorite added into 200 mL of CTAB solution with a concentration of 0.014 mol/L, and pH of the solutions was adjusted to 6.5 using 0.1 mol/L of NaOH solution. Then the solutions was transferred into a three-necked flask, which was then placed in a 70°C thermostat water bath for 24 h, after that, the product was repeatedly washed with deionized water until no Br^{-} remained, then dried at 80°C for 24 h, ground and screened with 200 mesh standard sieve, so the product REC-CTAB was obtained [17].

2.2.3. Preparation of Fe_3O_4/REC-CTAB composite

3.1 g of $FeCl_3{\cdot}6H_2O$ was dissolved with 50 mL of deionized water in beaker, then added 4 g of REC-CTAB and 1 g of PVP into the ferric chloride solution, stirred for 24 h to get a well-mixed solution. Then the mixture solution was transferred into a 500 mL three-necked flask, which was placed in a 60°C thermostat water bath. Then the Fe^{2+} solution was added into the three-necked flask, and at the same time, the mixture was stirred at the velocity of 600 rpm at 60°C to keep the mixture as sufficient suspension under N_2 atmosphere.

After 30 min, the stirring rate was decreased to 400 rpm followed by drop wise addition of $NH_3{\cdot}H_2O$ solution. After 90 min, stopped reaction, the mixture was held at 60°C for aging 120 min. Finally, the precipitates were collected by magnetic separation, and then washed with deionized water to neutral, washed with ethanol for several times to

remove PVP. The obtained Fe_3O_4/REC-CTAB composite was dried at 60°C for 24 h, ground and screened with 200 mesh standard sieve.

2.2.4. Assembly of the composite HA/CTS/Fe_3O_4/REC-CTAB

1.5 g of chitosan was added into 20 mL of 1% acetic acid aqueous solution (w/v). pH of the chitosan solution was adjusted to 4.9 using 0.1 M aqueous solution of NaOH. Then 0.5 g of HA and 0.35 g of Fe_3O_4/REC-CTAB were added into the chitosan solution under stirring condition. The solution was stirred for 1 h. The mixture was added dropwise using syringe into 1% STPP solution (w/v) whose pH is 4.0, so that small pellets were formed in STPP solution [18]. Then the pellets were allowed to age in the solution for 24 h, afterwards, the pellets were washed for 6–8 times to neutral, the obtained composite HA/CTS/Fe_3O_4/REC-CTAB was dried at 50°C for 12 h. The fabrication process of the composite catalyst is exhibited in Fig. 1.

2.3. Adsorption of heavy metals

Samples of the various adsorbates (Cd^{2+}, Pb^{2+} and Cu^{2+} ions) were prepared at various concentrations in aqueous solution. A fixed, known quantity of the dried composite HA/CTS/Fe_3O_4/REC-CTAB was then weighed into each of a series of conical flasks (150 mL capacity) and 50 mL of a particular concentration of a heavy metal ion solution added to each flask. After shaking for a known time at the rate of 150 rpm at 15°C, 25°C or 35°C, the samples were separated by centrifugation and the concentration of heavy metal ion remaining in the supernatant was determined by AA-6300 atomic absorption spectrophotometer (Shimadzu Instrument Co. Ltd., Japan).

2.4. Characterization of the composite

Scanning electron microscope (SEM): The composite HA/CTS/Fe_3O_4/REC-CTAB was stabilized in a sample holder, coated with gold, and observed with an S-4800 scanning electron microscope.

Transmission electron microscope (TEM): Fe_3O_4/REC-CTAB and HA/CTS/Fe_3O_4/REC-CTAB powders were dispersed in alcohol. Sample suspensions were dropped into a copper grid, dried under an infrared light, and tested with a Tecnai-12 transmission electron microscope (Netherlands PHILIPS Company).

X-ray diffraction (XRD): At room temperature, small angle diffraction was performed using X ray diffractometer with CuKα radiation (k = 0.154 nm), and the scanning rate was 1°/min, with a range of 2°–40°.

N_2 adsorption/desorption: Nitrogen adsorption/desorption isotherms and pore diameter distributions curve of HA/CTS/Fe_3O_4/REC-CTAB were determined at 77 K using ASAP-2020V3.4H N_2 adsorption/desorption instrument (Micromeritics Co. Ltd., USA).

Fourier transform infrared spectroscopy (FTIR) analysis: The sample powders were dispersed in KBr and pressed into transparent sheets for testing, in the spectral range of 400–4,000 cm^{-1} wavenumber.

The magnetic properties of REC, REC-CTAB, Fe_3O_4/REC-CTAB and HA/CTS/Fe_3O_4/REC-CTAB were measured in a Squid-vibrating sample magnetometer (VSM) magnetometer, in the range of –20,000 to +20,000 O_e.

3. Results and discussion

3.1. Characterization of the composite

3.1.1. Scanning electron microscope

Fig. 2a is the SEM image of REC, as can be seen from Fig. 2a, the surface of REC is smooth, showing obvious layered stacking structure.

Fig. 2b is the surface morphology of composite HA/CTS/Fe_3O_4/REC-CTAB, as shown in Fig. 2b, humic acid and chitosan were uniformly loaded on the surface of Fe_3O_4/REC-CTAB, and most of them are granulated, the structure

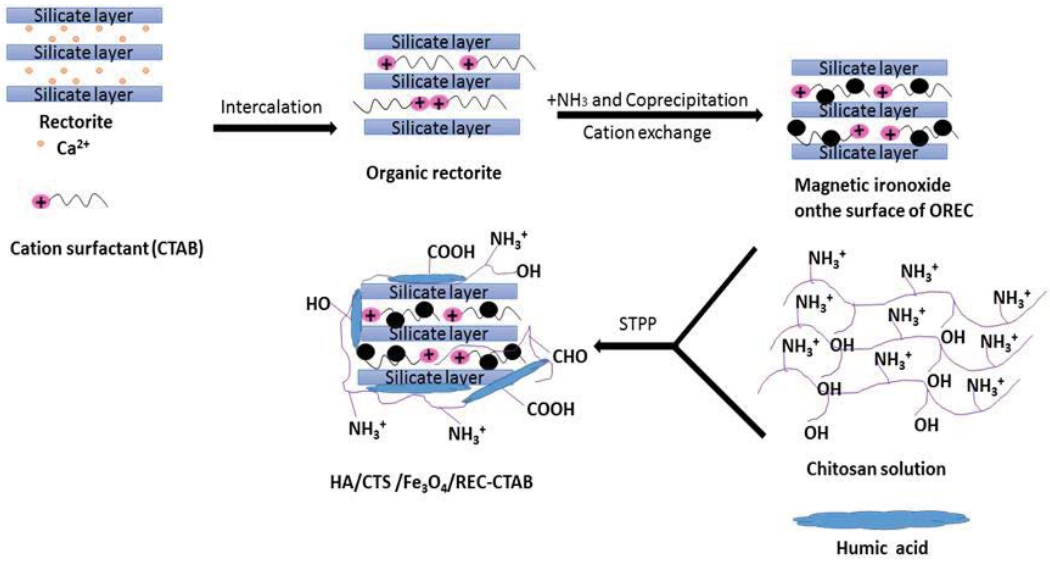

Fig. 1. Fabrication process of the composite HA/CTS/Fe_3O_4/REC-CTAB.

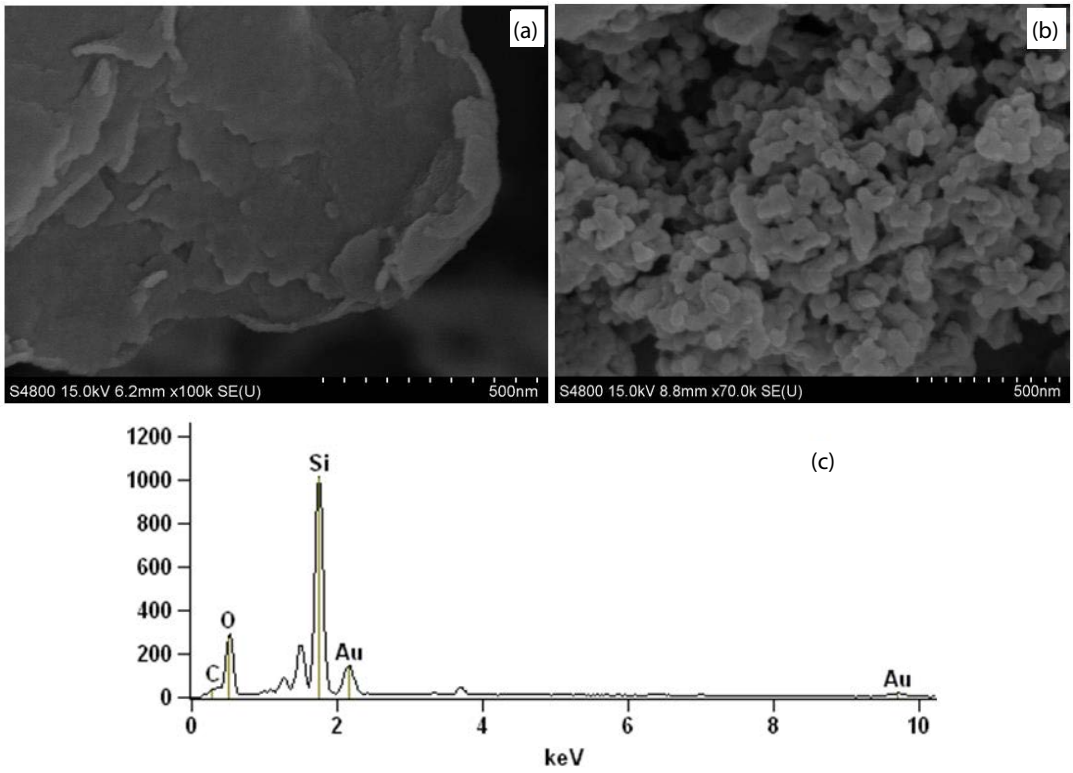

Fig. 2. (a) SEM image of REC, (b) SEM image of HA/CTS/Fe_3O_4/REC-CTAB, and EDS of HA/CTS/Fe_3O_4/REC-CTAB.

is loose, indicating that the composite adsorbent is more easier to adsorb pollutant than rectorite.

Fig. 2c is the elemental energy spectrum of the composite HA/CTS/Fe_3O_4/REC-CTAB, the peaks of element C, Si and O can be clearly found in Fig. 2c, and no miscellaneous peaks appeared, indicating that there are no other substances doped or contaminated in the samples.

3.1.2. Transmission electron microscope

Fig. 3a shows the TEM micrograph of the composite Fe_3O_4/REC-CTAB, it is seen from Fig. 3a that Fe_3O_4 is intercalated into the interlayer spaces of rectorite evenly with a diameter of about 15–20 nm.

Fig. 3b is the TEM micrograph of the composite HA/CTS/Fe_3O_4/REC-CTAB, it can be observed from Fig. 3b that the surface of the composite is irregular and the flocculent aggregated structure appeared, indicating that chitosan and humic acid on the surface can form a reticular structure via cross-linking. Therefore, it can be confirmed that the inorganic–organic composite was formed by using magnetic rectorite, humic acid and chitosan.

3.1.3. X-ray diffraction

Fig. 4a illustrates the small-angle diffraction XRD spectra of REC, REC-CTAB, Fe_3O_4/REC-CTAB and HA/CTS/Fe_3O_4/REC-CTAB, data sets were arranged over the range of 2°–10°.

As shown in Fig. 4a, raw rectorite displayed two diffraction peaks located at 2θ = 3.86° and 7.9°, belonging to crystal plane R (001) and R (002), respectively. According to the Bragg diffraction equation $\lambda = 2d\sin\theta$ [19], the distance of interlayer space of REC (d 001 and d 002) can be calculated as approximately 2.29 and 1.12 nm. After being modified by CTAB, the diffraction peak of crystal plane R (001) of REC-CTAB shifted to 2θ = 3.04°, and the distance of interlayer space was extended to 3.05 nm. Moreover, the diffraction peak of R (002) disappeared. These indicated that CTAB was successfully intercalated into the interlayer space of REC, and cationic exchange reaction occurred between REC and CTAB [9].

As shown in Fig. 4a, compared with REC-CTAB, the diffraction peak of the crystal plane R (001) of Fe_3O_4/REC-CTAB is weakened after the intercalation of iron oxide into the interlayer space of REC-CTAB, indicating that cationic exchange reaction occurred between Fe^{3+} (or Fe^{2+}) and Na^+ in the interlayer space of REC and deposited some Fe_3O_4 particles on the surface of REC. Moreover, the intensity of diffraction peak of R (002) is obviously weakened. This indicates that the introduction of Fe_3O_4 damages the ordered structure of some REC, resulting in the REC layer structure being intercalated or stripped to a different extent. It can also be seen from Fig. 4a that the diffraction peaks of the composite HA/CTS/Fe_3O_4/REC-CTAB are all very weak, this is because HA is loaded on the surface of the composite and the diffraction peaks are covered.

As shown in Fig. 4b, the characteristic diffraction peaks of Fe_3O_4/REC-CTAB located at 2θ = 35.7° is related to (311) crystal planes of face-centered cubic Fe_3O_4, which is also observed in the diffraction pattern of HA/CTS/Fe_3O_4/REC-CTAB, confirming that iron oxide has been intercalated into the interlayer space of REC [9,20].

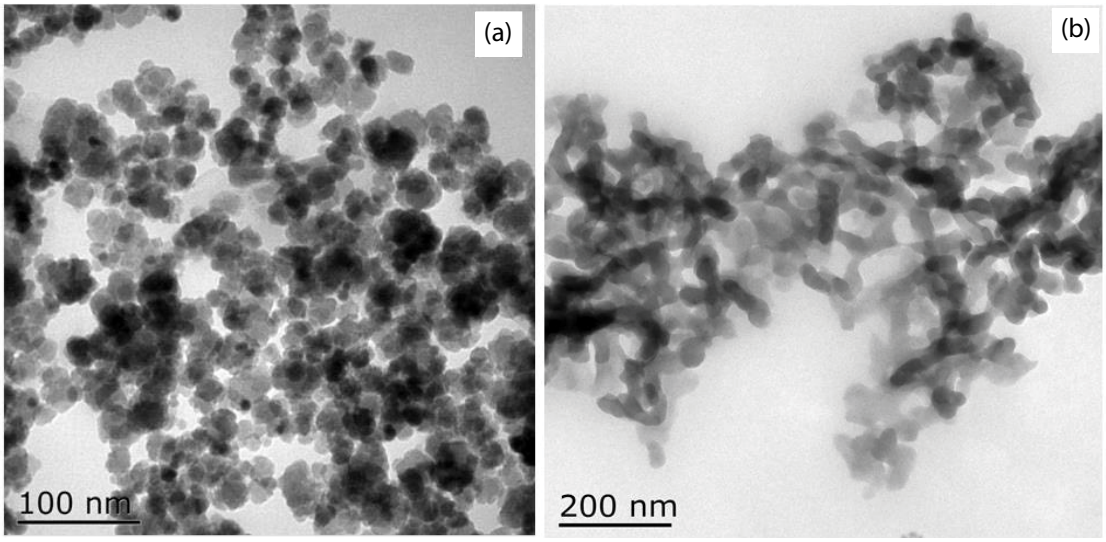

Fig. 3. (a) TEM micrographs of Fe_3O_4/REC-CTAB and (b) HA/CTS/Fe_3O_4/REC-CTAB.

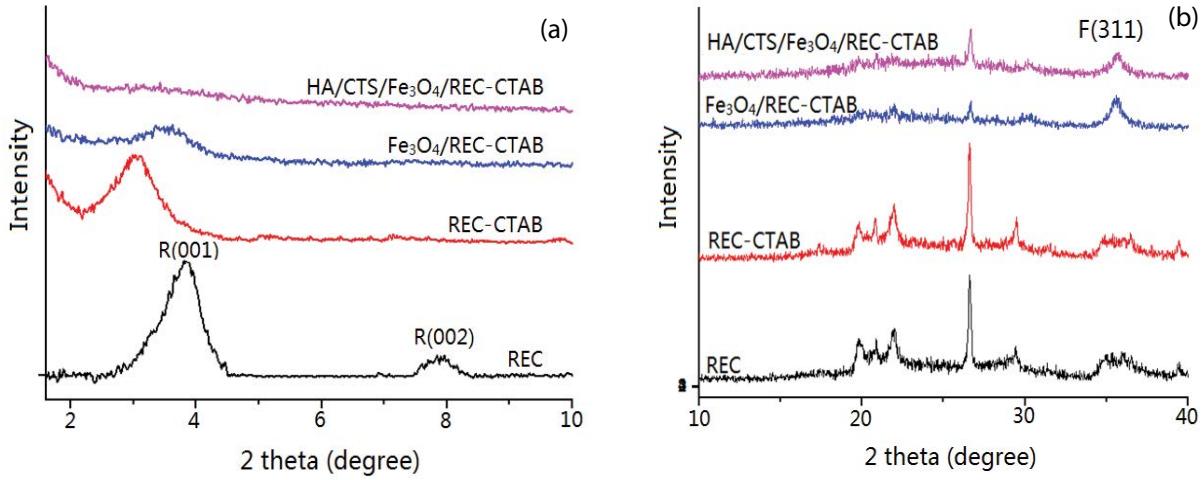

Fig. 4. X-ray diffraction peaks of REC, REC-CTAB, Fe_3O_4/REC-CTAB and HA/CTS/Fe_3O_4/REC-CTAB, (a) from 1° to 10° and (b) from 10° to 40°.

3.1.4. N_2-BET test

The nitrogen adsorption–desorption isotherms and BJH pore size distribution curve measured at 77 K for the composite HA/CTS/Fe_3O_4/REC-CTAB are depicted in Figs. 5a and b.

From nitrogen adsorption–desorption isotherms shown in Fig. 5a, according to BET principle, the specific surface area of the composite adsorbent HA/CTS/Fe_3O_4/REC-CTAB was calculated as 24.11 m^2/g.

From differential distribution curve of pore size shown in Fig. 5b, the average pore diameter and pore volume of the composite adsorbent HA/CTS/Fe_3O_4/REC-CTAB was calculated as 16.48 nm and 0.094 cm^3/g, respectively.

The specific surface area of HA/CTS/Fe_3O_4/REC-CTAB is larger than that of raw REC, this is probably attributed to the dispersion of HA particles with larger surface area on the surface of Fe_3O_4/REC-CTAB [21].

The adsorption–desorption isotherms shown in Fig. 5a resemble type IV isotherm, in accordance with the International Union of Pure and Applied Chemistry (IUPAC) classification. Type IV isotherm usually exhibits a rapid increase of adsorption capacity at low relative pressure, indicating that there exist unrestricted monolayer and multilayer adsorption.

It can be seen from the isotherms that the monolayer coverage completed at the relative pressure ranges up to 0.45 [22]. The pore size distribution curves depicted in Fig. 5b shows that the composite HA/CTS/Fe_3O_4/REC-CTAB is a mesoporous material.

3.1.5. Vibrating sample magnetometer

The hysteresis loop is measured at room temperature using the SQUID-VSM magnetic measurement system produced by American company of Duantum Design.

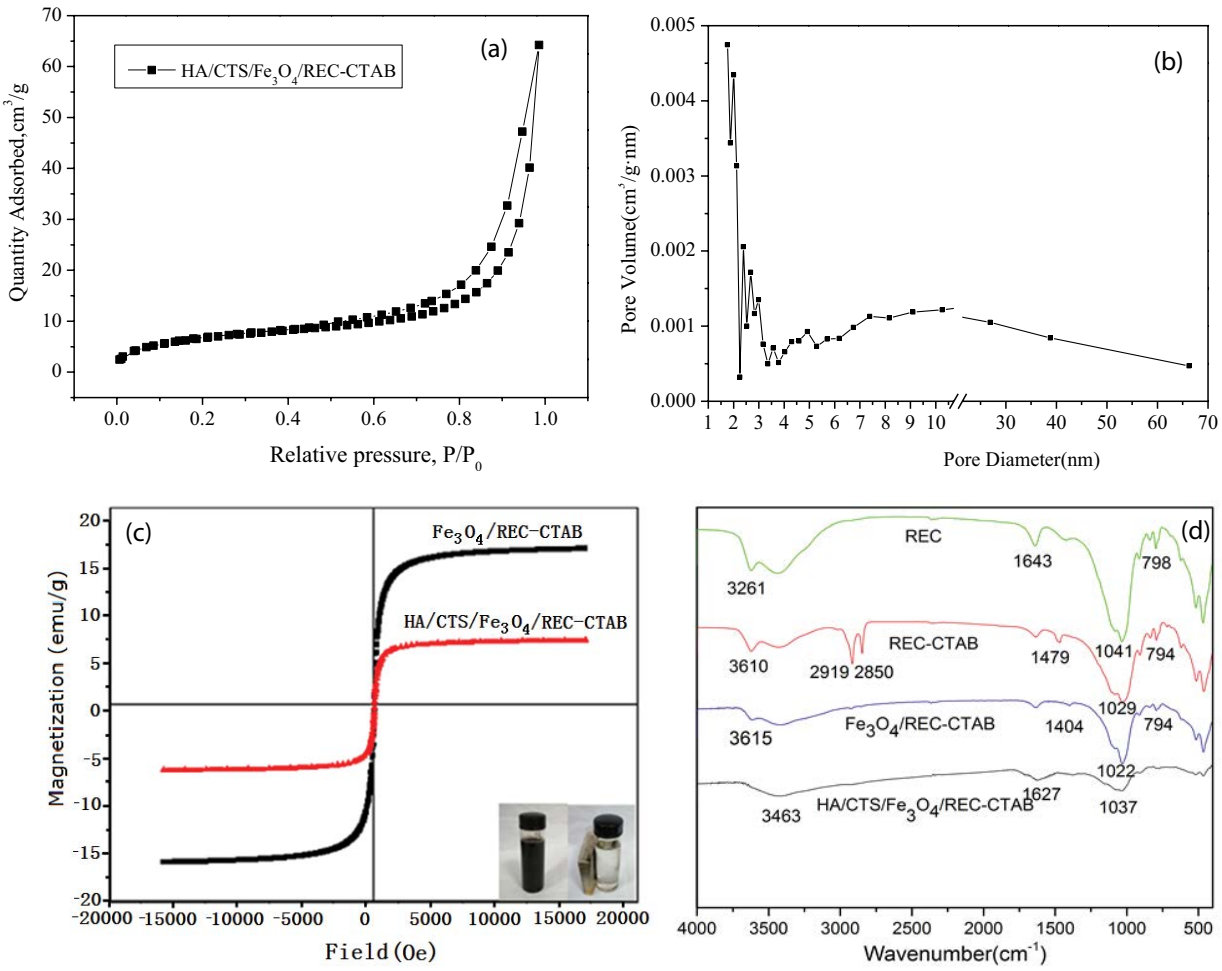

Fig. 5. Nitrogen adsorption/desorption isotherms (a), BJH pore diameter distributions (b), magnetic hysteresis loop (c) and FTIR spectra (d) of HA/CTS/Fe_3O_4/REC-CTAB.

The Fe_3O_4/REC-CTAB was used as a reference for evaluation of magnetic performance of HA/CTS/Fe_3O_4/REC-CTAB, the measured hysteresis loop is shown in Fig. 5c.

As can be seen from Fig. 5c, for the composite material Fe_3O_4/REC-CTAB and HA/CTS/Fe_3O_4/REC-CTAB, with the increase of the magnetic field strength, the internal magnetic domain increases continuously and the magnetization also increases gradually until the saturation magnetization is reached. When the applied magnetic field reaches to ±20,000 Oe, the saturation magnetization of Fe_3O_4/REC-CTAB is 19.9 emu/g, while the saturation magnetization of HA/CTS/Fe_3O_4/REC-CTAB is 6.6 emu/g. From the magnetization curve shown in Fig. 5c, the coercivity and remanence of the composite HA/CTS/Fe_3O_4/REC-CTAB are nearly zero, indicating that the composite was a superparamagnetic material [20,23]. When used, the phenomenon of magnetic aggregation of HA/CTS/Fe_3O_4/REC-CTAB did not occur, indicating that HA/CTS/Fe_3O_4/REC-CTAB prepared is easily separated from aqueous solution under appropriate applied magnetic field and magnetic field gradient.

As can be seen from Fig. 5c, the composite adsorbent HA/CTS/Fe_3O_4/REC-CTAB is hard to be separated from aqueous solution when the magnetic field is not furnished. But, after being dispersed into the solutions, under the action of the magnetic field, the composite adsorbent was rapidly migrated directionally to be aggregated on the side of the magnet. After a few minutes of magnetic separation, the solution is clarified.

3.1.6. Fourier-transform infrared spectroscopy

The FTIR spectra of REC, REC-CTAB, Fe_3O_4/REC-CTAB and HA/CTS/Fe_3O_4/REC-CTAB are shown in Fig. 5d.

From Fig. 5d we can see, in FTIR spectra of REC, the absorption band at 3,261 cm^{-1} was related to the hydroxyl stretching bond of Si–O–H [9]. The absorption band at 1,041 cm^{-1} was associated to thein-plane Si–O–Si stretching vibration, and the absorption band at 798 cm^{-1} was due to Si–O–Al bending vibration. These absorption bands also appeared in the FTIR spectra of REC-CTAB, Fe_3O_4/REC-CTAB and HA/CTS/Fe_3O_4/REC-CTAB. After REC was modified by CTAB, there appeared two new absorption bands at 2,850 and 2,919 cm^{-1} for REC-CTAB. These new absorption bands were attributed to the symmetric and asymmetric stretching vibration of CH^{2-} [20]. However, these two absorption bands disappeared in the FTIR spectra of Fe_3O_4/REC-CTAB and

HA/CTS/Fe_3O_4/REC-CTAB, indicating that CH^{2-} stretching vibration is weakened, which is due to the overlapping of Fe_3O_4 and CTAB to enable the effect of CTAB weakened.

3.2. Adsorption of Cu^{2+}, Cd^{2+} and Pb^{2+} onto composite adsorbent HA/CTS/Fe_3O_4/REC-CTAB

3.2.1. Effect of initial pH of the heavy metal ions aqueous solution on the adsorption

To evaluate the influence of pH of the heavy metal ions aqueous solution on the adsorption function alone, the critical pH values below which the three kinds of cations could not be precipitated from solution were calculated. It was found that for initial concentration of Cu^{2+}, Cd^{2+} and Pb^{2+} ions equal to 10 mg/L, the critical pH values were 6.45, 9.20, 10.30 for Cu^{2+}, Cd^{2+} and Pb^{2+} ions, respectively. Over these critical pH ranges, the plots of the relationship between the adsorption capacities of Cu^{2+}, Cd^{2+} and Pb^{2+} ions and the pH value may be represented in the manner shown in Fig. 6.

As can be seen from Fig. 6, the initial pH value of the heavy metal ions aqueous solution had a considerable influence on the removal rates of Cu^{2+}, Cd^{2+} and Pb^{2+} ions from the solutions, with the removal rate for all three kinds of heavy metal ions increasing as pH value increased. When pH values were 5.0~6.5, the adsorptive capacities reached the larger values. There exist many carboxyl groups on the surface of the composite adsorbent. The acidic solution can inhibit dissociation of the carboxyl group, so most of the carboxyl groups exist in the form of –COOH; the adsorptive active sites which generate electrostatic gravitation to heavy metal ions were reduced, resulting in lower adsorption capacity. At pH values above the range 5.0–6.5, the adsorption capacities of the heavy metal ions increased at slower rate because of competitive adsorption between hydrogen ions and the heavy metal cations. Therefore, because the concentration of hydrogen ions decreased as the pH increases, the adsorption capacities continued to increase with increasing pH value.

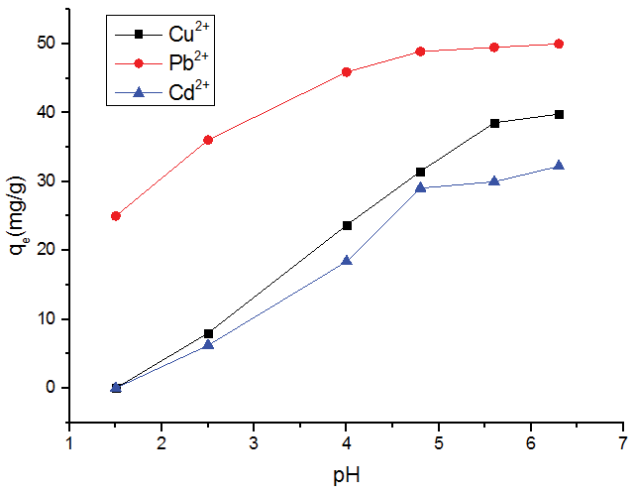

Fig. 6. Effect of initial pH of the heavy metal ions aqueous solution on the adsorption. Conditions: temperature, 35°C; mass of adsorbent, 0.01 g; volume of solution, 50 mL; initial concentration of heavy metal ions Cu^{2+}, Cd^{2+} and Pb^{2+} is 10 mg/L.

3.2.2. Adsorption isotherms

Adsorption isotherms of the three heavy metal ions on the composite adsorbent are shown in Fig. 7.

The shape of the adsorption isotherm shown in Fig. 7 can be described as type L2 according to the classification given by Giles et al. [24]. The data obtained may be fitted to the Langmuir and Freundlich models.

The Langmuir model is based on the formation of an ideal monomolecular layer adsorption, and the linear form of the model can be expressed as follows:

$$\frac{C_e}{q_e} = \frac{1}{q_0 b} + \frac{C_e}{q_0} \tag{1}$$

where q_e (mg/g) is the equilibrium adsorption capacity; q_0 (mg/g) is the saturation adsorption capacity attained; C_e (mg/L) is the concentration of adsorbate aqueous solution at equilibrium; b (L/mg) is the Langmuir adsorption equilibrium constant.

Langmuir isotherms in the form of plots of C_e/q vs. C_e according to Eq. (1) were all linear for the experimental data reported as Fig. 7. The fitted results obtained via the Langmuir model are listed in Table 1.

From Table 1 given, we can see that the adsorption of Cu^{2+}, Cd^{2+} and Pb^{2+} ions on the composite adsorbent HA/CTS/Fe_3O_4/REC-CTAB prepared can be described by the Langmuir model.

The adsorption can be classified as the monomolecular layer type. The data listed in Table 1 show that the saturated adsorption capacity q_0 increased as the temperature increased for the adsorption of the three heavy metal ions, indicating that the adsorption process is endothermic, and the mechanism for adsorption of Cu^{2+}, Cd^{2+} and Pb^{2+} involves chemical bonding, that is, the amino and hydroxyl groups on chitosan molecule and hydroxyl and carboxyl groups on humic acid molecule surface chelated with three metal ions, or exchangeable ions on rectorite surface exchanged with these metal ions.

A list for the comparison of saturation monolayer adsorption capacities (q_0) of Cu^{2+}, Cd^{2+} and Pb^{2+} metal ions on different adsorbents is given in Table 2 [25–37]. The saturation monolayer adsorption capacity of the composite adsorbent HA/CTS/Fe_3O_4/REC-CTAB prepared was higher than other adsorbents shown in Table 2. Furthermore, more value of q_0 for Pb^{2+} than Cu^{2+} and Cd^{2+} was due to higher binding capacity of Pb^{2+} with the composite adsorbent HA/CTS/Fe_3O_4/REC-CTAB prepared.

The linear form of the Freundlich model is given as follows:

$$\log q_e = \log k + \frac{1}{n}\log C_e \tag{2}$$

where k and n are Freundlich characteristic constant, and q_e and C_e have the same meanings as mentioned above.

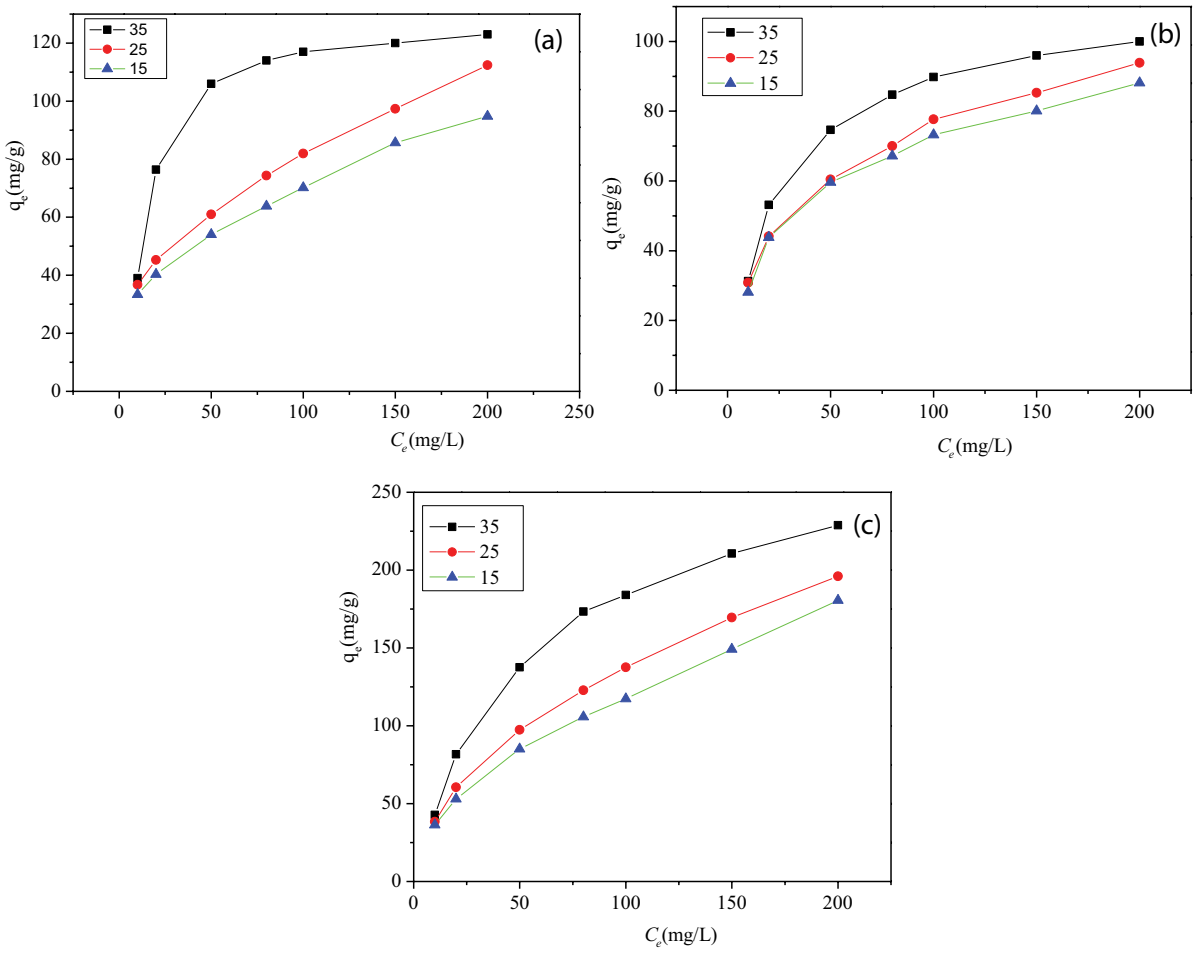

Fig. 7. Adsorption isotherms for Cu^{2+} (a), Cd^{2+} (b) and Pb^{2+} (c). Conditions: temperature, 35°C; mass of adsorbent, 0.01 g; volume of solution, 50 mL; initial concentration of Cu^{2+}, Cd^{2+} and Pb^{2+} aqueous solutions, 10 mg/L.

Table 1
Fit of linear results to the Langmuir model

Heavy metal cation	Temperature (°C)	q_0	b	Correlation coefficient (R^2)
	15	107.76	0.02499	0.9827
Cu^{2+}	25	128.04	0.02291	0.9537
	35	134.77	0.05782	0.9965
	15	97.847	0.03381	0.9922
Cd^{2+}	25	105.15	0.03132	0.9895
	35	111.98	0.04059	0.9996
	15	209.90	0.01514	0.9445
Pb^{2+}	25	221.24	0.01866	0.9786
	35	279.33	0.02093	0.9972

Freundlich isotherms in the form of plots of log q_e vs. log C_e according to Eq. (2) were all linear for the experimental data reported as Fig. 7. The fitted results obtained via the Freundlich model are listed in Table 3.

From Table 3 we can see that the adsorption of Cu^{2+}, Cd^{2+} and Pb^{2+} ions on the composite adsorbent HA/CTS/Fe_3O_4/REC-CTAB prepared can be described by the Freundlich model.

The values of $1/n$ listed in Table 3 were found to lay in the range 0.1–0.5, indicating that all three kinds of heavy metal cations were readily adsorbed by the composite adsorbent HA/CTS/Fe_3O_4/REC-CTAB obtained [38].

3.2.3. Adsorption kinetics

Fig. 8 reveals the adsorption rate curves of the three kinds of heavy metal ions on the composite adsorbent HA/CTS/Fe_3O_4/REC-CTAB.

From Fig. 8 we can see that all of the adsorption took 4 h to reach the equilibrium.

At present study, the adsorption kinetics data shown in Fig. 8 are simulated using pseudo-first-order dynamics and pseudo-second-order kinetics models [6]. The linear form of pseudo-first-order and pseudo-second-order kinetics equation can be represented as follows:

$$\ln(q_e - q_t) = \ln q_e - K_1 t \tag{3}$$

$$\frac{t}{q_t} = \frac{1}{K_2 q_e^2} + \frac{t}{q_e} \tag{4}$$

Table 2
Comparison of saturation monolayer adsorption capacity of Cu^{2+}, Cd^{2+} and Pb^{2+} ions using various adsorbents

Metal ion	Adsorbents	Maximum monolayer Adsorption capacity (ma/g)	References
Cu^{2+}	Nano-composite adsorbent	173.62	[25]
	Layered double hydroxide-humic hybrid	47.63	[26]
	Magnetic graphene oxide composite	62.73	[27]
	Ploy(MVE-alt-MA-1)	81.72	[28]
	Composite adsorbent HA/CTS/Fe_3O_4/REC-CTAB	128.04	Present work
Cd^{2+}	YVO_4:Eu^{3+} nanoparticles	99.01	[29]
	EGTA dianhydride modified ramie fiber	159.11	[30]
	Adsorbent from mixture of bagasse-bentonite	20.62	[31]
	Modified bamboo charcoal	6.65	[32]
	Composite adsorbent HA/CTS/Fe_3O_4/REC-CTAB	105.15	Present work
Pb^{2+}	Chitosan/magnetic nanocomposite beads	63.3	[33]
	SDS-AZS	18.38	[34]
	Ti(IV) iodovanadate cation exchanger	63.29	[35]
	EDTA-Zr(IV) iodate composite cation exchanger	26.04	[36]
	PSTM nanocomposite cation exchanger	30.58	[37]
	Composite adsorbent HA/CTS/Fe_3O_4/REC-CTAB	221.24	Present work

Table 3
Fit of linear results to the Freundlich model

Heavy metal cation	Temperature (°C)	k	$1/n$	Correlation coefficient (R^2)
Cu^{2+}	15	3.1737	0.3505	0.9909
	25	3.2433	0.3710	0.9926
	35	3.8451	0.3525	0.8395
Cd^{2+}	15	3.7472	0.3620	0.9716
	25	3.1598	0.3635	0.9901
	35	3.2923	0.3728	0.9329
Pb^{2+}	15	3.5201	0.4994	0.9979
	25	3.1823	0.4868	0.9856
	35	2.9027	0.4975	0.9722

where q_e (mg/g) is the equilibrium adsorption capacity; q_t (mg/g) is the amounts of metal ion adsorbed at any time t (min); K_1 is the pseudo-first-order apparent adsorption rate constant; K_2 is the pseudo-second-order apparent adsorption rate constant.

The data shown in Fig. 8 were fitted by pseudo-first-order and pseudo-second-order models, the fitted results are listed in Table 4.

As shown in Table 4, when the pseudo-first-order kinetic equation was used to fit the adsorption rate experimental data, the correlation was poor. So, the adsorption process of the three heavy metal ions on the composite adsorbents prepared could not be described by the pseudo-first-order equation. However, the pseudo-second-order kinetic model can better match the experimental data, and the correlation is very good.

The equilibrium adsorption capacity of Cu^{2+}, Cd^{2+} and Pb^{2+} on the composite adsorbent at 35°C calculated according

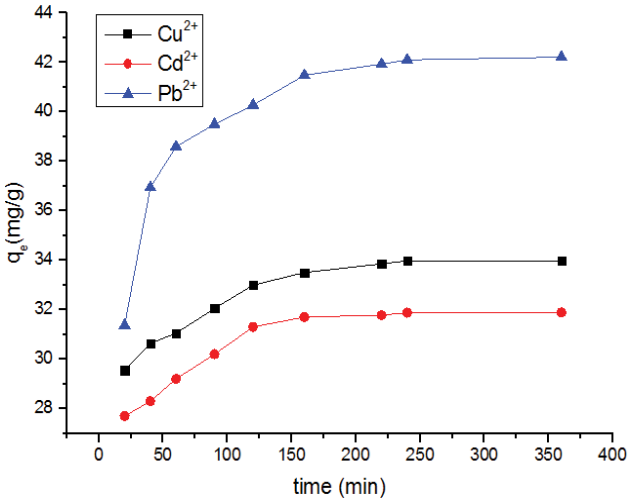

Fig. 8. Adsorption rate curve of Cu^{2+}, Cd^{2+} and Pb^{2+}on to HA/CTS/Fe_3O_4/REC-CTAB. Conditions: temperature 35°C; mass of adsorbent, 0.01 g; volume of heavy metal ion aqueous solution, 50 mL; concentration of heavy metal ion aqueous solution, 10 mg/L.

to the pseudo-second-order kinetic model was 39.54, 35.32 and 50.89 mg/g, respectively, which was close to the actual equilibrium adsorption capacity (Fig. 8). Therefore, the adsorption process of the three heavy metal ions on the composite adsorbent follows the pseudo-second-order kinetics equation.

3.2.4. Regeneration of the adsorbent

0.1 M of HCl aqueous solution was used as regenerative agent to desorb the heavy metal ions adsorbed on the

Table 4
Fitted results to the pseudo-first-order and pseudo-second-order models

Cation	Pseudo-first-order			Pseudo-second-order		
	K_1 (1/min)	$q_{e,cal}$ (mg/g)	R^2	q_e (mg/g)	K_2 (g/mg/min)	R^2
Cu^{2+}	0.0002247	7.413	0.7341	39.54	0.001178	0.9986
Cd^{2+}	0.0002271	7.168	0.6698	35.32	0.001351	0.9991
Pb^{2+}	0.0009319	11.22	0.6485	50.89	0.0004828	0.9993

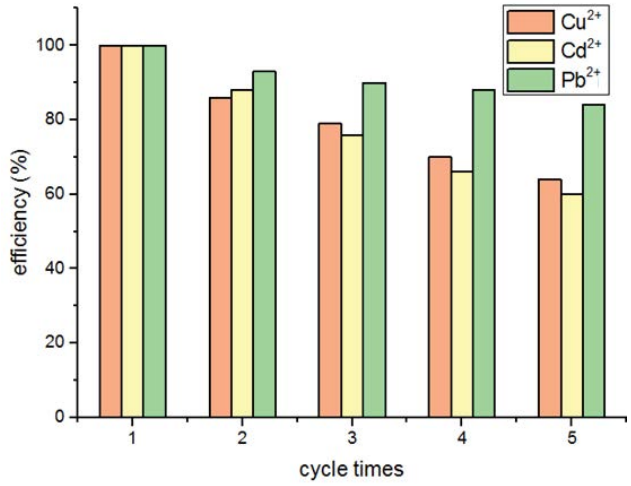

Fig. 9. Five consecutive adsorption cycles of HA/CTS/Fe_3O_4/REC-CTAB for Cu^{2+}, Cd^{2+} and Pb^{2+}.

composite adsorbent. The composite adsorbent desorbed is then used to adsorb the three heavy metal ions again. Five consecutive adsorption cycles were investigated, the results are shown in Fig. 9.

The results shown in Fig. 9 proved that the three heavy metal ions can effectively be desorbed from the adsorbent. The adsorption efficiency of the three heavy metal ions decreased with the increase of adsorption cycles, which may be due to the loss of adsorbent in the process of reuse. The adsorption efficiency of Cu^{2+}, Cd^{2+} and Pb^{2+} on regenerated HA/CTS/Fe_3O_4/REC-CTAB decreased to 64.0%, 60.0% and 84.0% at the fifth time, respectively. However, after being used for five times, the composite adsorbent HA/CTS/Fe_3O_4/REC-CTAB has still better adsorption properties. The results show that the regenerative properties of the composite adsorbents are better and can be reused many times.

4. Conclusion

After the rectorite being modified using CTAB, Fe_3O_4 particles were introduced into the expanded interlayer spacing of the rectorite, and HA and CTS were loaded on the surface of Fe_3O_4/REC-CTAB by sol-gel method; finally, the magnetic composite adsorbent (HA/CTS/Fe_3O_4/REC-CTAB) could be successfully prepared. The composite adsorbent obtained is a kind of mesoporous material with high specific surface area. Compared with raw rectorite (REC), the material has excellent adsorptive properties for Cu^{2+}, Cd^{2+} and Pb^{2+} in aqueous solution. The isothermal adsorption process for each ion can be well described by the Freundlich and Langmuir models, and the adsorption kinetics conforms to the pseudo-second-order kinetics equation.

The composite material exhibited superparamagnetic behavior with small coercivity in the applied magnetic fields, and can be quickly separated from aqueous phase after being used under suitable applied magnetic field and magnetic field gradient.

In addition, the adsorbent HA/CTS/Fe_3O_4/REC-CTAB used could be regenerated by HCl aqueous solution and remained a good adsorptive performance to be reused many times. This foreshadowed a broad application prospect of HA/CTS/Fe_3O_4/REC-CTAB.

Acknowledgments

This work was supported by Zhangjiagang Science and Technology Support Program (Social Development) of Jiangsu Province, China (grant numbers: ZKS1510).

References

[1] D.L. Wu, P.W. Zheng, P.R. Chang, X.F. Ma, Preparation and characterization of magnetic rectorite/iron oxide nanocomposites and its application for the removal of the dyes, Chem. Eng. J., 174 (2011) 489–494.
[2] G. Sharma, B. Thakur, Mu. Naushad, A.H. Al-Muhtaseb, A. Kumar, M. Sillanpaa, G.T. Mola, Fabrication and characterization of sodium dodecyl sulphate@ironsilicophosphate nanocomposite: ion exchange properties and selectivity for binary metal ion, Mater. Chem. Phys., 193 (2017) 129–139.
[3] G. Sharma, B. Thakur, Mu. Naushad, A. Kumar, F.J. Stadler, S.M. Alfadul, G.T. Mola, Applications of nanocomposite hydrogels for biomedical engineering and environmental protection, Environ. Chem. Lett., 16 (2018) 113–146.
[4] L.H. Luo, The Preparation and Applied in Wastewater Treatment of Magnetic Rectorite Composite Materials, Master's Degree Thesis of Southwest University of Science and Technology, Mianyang city, Sichuan province, China, 2011.
[5] H.C. Liu, W. Chen, C. Liu, Y. Liu, C.L. Dong, Magnetic mesoporous clay adsorbent: preparation, characterization and adsorption capacity for atrazine, Microporous Mesoporous Mater., 194 (2014) 72–78.
[6] M.J. Xie, L.X. Zeng, Q.Y. Zhang, Y. Kang, H.J. Xiao, Y.N. Peng, X.C. Chen, J.W. Luo, Synthesis and adsorption behavior of magnetic microspheres based on chitosan/organic rectorite for low-concentration heavy metal removal, J. Alloys Compd., 647 (2015) 892–905.
[7] P.P. Chang, X.K. Wang, S.M. Yu, W.S. Wu, Sorption of Ni(II) on Na-rectorite from aqueous solution: effect of pH, ionic strength and temperature, Colloids Surf., A, 302 (2007) 75–81.
[8] Y. Zhao, Z.Y. Shao, C.L. Chen, J. Hu, H.L. Chen, Effect of environmental conditions on the adsorption behavior of Sr(II) by Na-rectorite, Appl. Clay Sci., 87 (2014) 1–6.

[9] F. Wang, D. Liu, P.W. Zheng, X.F. Ma, Synthesis of rectorite/Fe_3O_4-CTAB composite for the removal of nitrate and phosphate from water, J. Ind. Eng. Chem., 41 (2016) 165–174.
[10] H.L. Hong, W.-T. Jiang, X.L. Zhang, L.Y. Tie, Z.H. Li, Adsorption of Cr(VI) on STAC-modified rectorite, Appl. Clay Sci., 42 (2008) 292–299.
[11] S. Babel, T.A. Kurniawan, Low-cost adsorbents for heavy metals uptake from contaminated water: a review, J. Hazard. Mater., 97 (2003) 219–243.
[12] C.A. Caro, L. Lillo, F.J. Valenzuela, G. Cabello, Mechanistic characterization and inhibition of sphingomyelinase C over substituted Iron Schiff bases of chitosan adsorbed on glassy carbon electrode, Chem. Biol. Interact., 263 (2017) 81–87.
[13] Z.L. Deng, J. Jung, Y.Y. Zhao, Development, characterization, and validation of chitosan adsorbed cellulose nanofiber (CNF) films as water resistant and antibacterial food contact packaging, LWT Food Sci. Technol., 83 (2017) 132–140.
[14] F.M. Goycoolea, V. Milkova, Electrokinetic behavior of chitosan adsorbed on o/w nanoemulsion droplets, Colloids Surf., A, 519 (2017) 205–211.
[15] W.S.W. Ngah, L.C. Teong, M.A.K.M. Hanafiah, Adsorption of dyes and heavy metal ions by chitosan composites: a review, Carbohydr. Polym., 83 (2011) 1446–1456.
[16] J. Zhang, W.X. Hu, Z.Q. Zhang, Study on the orgranophilic modification of rectorite, J. Wuhan Inst. Chem. Technol., 27 (2005) 35–37.
[17] Y. Wang, C. Sun, X. Sun, J. Hinkley, G.M. Odegard, T.S. Gates, 2-D nano-scale finite element analysis of a polymer field, Compos. Sci. Technol., 63 (2003) 1581–1590.
[18] V. Arya, L. Philip, Adsorption of pharmaceuticals in water using Fe_3O_4 coated polymer clay composite, Microporous Mesoporous Mater., 232 (2016) 273–280.
[19] C.D. Delhom, L.A. White-Ghoorahoo, S.S. Pang, Development and characterization of cellulose/clay nanocomposites, Composites Part B, 41 (2010) 475–481.
[20] L. Zeng, M. Xie, Q. Zhang, Y. Kang, X. Guo, H. Xiao, Y. Peng, J. Luo, Chitosan/organic rectorite composite for the magnetic uptake of methylene blue and methyl orange, Carbohydr. Polym., 123 (2015) 89–98.
[21] R. Zhang, P. Zheng, X. Ma, Preparation and catalytic properties of magnetic rectorite-chitosan-Au composites, J. Alloys Compd., 690 (2017) 381–389.
[22] T.M. Budnyak, E.S. Yanovska, O.Y. Kichkiruk, D. Sternik, V.A. Tertykh, Natural minerals coated by biopolymer chitosan: synthesis, physicochemical, and adsorption properties, Nanoscale Res. Lett., 11 (2016) 492.
[23] J.J. Li, X. Bao, X.F. Wu, I. Nazrul, Y. Liu, S.Y. Qiao, Magnetic chitosan micron spheres: synthesis and adsorption property for Cu^{2+}, Chin. J. Inorg. Chem., 33 (2017) 383–388.
[24] C. Giles, D. Smith, General treatment and classification of the solute sorption isotherms, J. Colloid Interface Sci., 47 (1974) 755–765.
[25] M.R. Awual, G.E. Eldesoky, T. Yaita, Mu. Naushad, H. Shiwaku, Z.A. AlOthman, S. Suzuki, Schiff based ligand containing nanocomposite adsorbent for optical copper(II) ions removal from aqueous solutions, Chem. Eng. J., 279 (2015) 639–647.
[26] M.A. González, I. Pavlovic, R. Rojas-Delgado, C. Barriga, Removal of Cu^{2+}, Pb^{2+} and Cd^{2+} by layered double hydroxide–humate hybrid. Sorbate and sorbent comparative studies, Chem. Eng. J., 254 (2014) 605–611.
[27] X.-j. Hu, Y.-g. Liu, H. Wang, A.-w. Chen, G.-m. Zeng, S.-m. Liu, Y.-m. Guo, X. Hu, T.-t. Li, Y.-q. Wang, L. Zhou, S.-h. Liu, Removal of Cu(II) ions from aqueous solution using sulfonated magnetic graphene oxide composite, Sep. Purif. Technol., 108 (2013) 189–195.
[28] M. Ceglowski, G. Schroeder, Preparation of porous resin with Schiff base chelating groups for removal of heavy metal ions from aqueous solutions, Chem. Eng. J., 263 (2015) 402–411.
[29] Mu. Naushad, A.A. Ansari, Z.A. ALOthman, J. Mittal, Synthesis and characterization of YVO_4:Eu^{3+} nanoparticles: kinetics and isotherm studies for the removal of Cd^{2+} metal ion, Desal. Wat. Treat., 57 (2016) 2081–2088.
[30] Z.C. Sun, Y.G. Liu, Y.Q. Huang, X.F. Tan, G.M. Zeng, X.J. Hu, Z.Z. Yang, Fast adsorption of Cd^{2+} and Pb^{2+} by EGTA dianhydride (EGTAD) modified ramie fiber, J. Colloid Interface Sci., 434 (2014) 152–158.
[31] E.P. Kuncoro, D.R.M. Isnadina, H. Darmokoesoemo, F. Dzembarahmatiny, K.S. Kusuma, Characterization and isotherm data for adsorption of Cd^{2+} from aqueous solution by adsorbent from mixture of bagasse-bentonite, Data Brief, 16 (2018) 354–360.
[32] W.L. Li, Y.Q. Chen, J.Y. Wang, L. Lin, J. Yin, J.J. Tang, Study on adsorption of Cd^{2+} by modified bamboo charcoal, Adv. Mater. Res., 955–959 (2014) 2559–2563.
[33] H.V. Tran, L.D. Tran, T.N. Nguyen, Preparation of chitosan/magnetite composite beads and their application for removal of Pb(II) and Ni(II) from aqueous solution, Mater. Sci. Eng., C, 30 (2010) 304–310.
[34] M. Naushad, Surfactant assisted nano-composite cation exchanger: development, characterization and applications for the removal of toxic Pb^{2+} from aqueous medium, Chem. Eng. J., 235 (2014) 100–108.
[35] Mu. Naushad, Z.A. ALOthman, M.R. Awual, M.M. Alam, G.E. Eldesoky, Adsorption kinetics, isotherms, and thermodynamic studies for the adsorption of Pb^{2+} and Hg^{2+} metal ions from aqueous medium using Ti(IV) iodovanadate cation exchanger, Ionics, 21 (2015) 2237–2245.
[36] M. Naushad, Z.A. ALOthman, Inamuddin, H. Javadian, Removal of Pb(II) from aqueous solution using ethylene diamine tetra acetic acid-Zr(IV) iodate composite cation exchanger: kinetics, isotherms and thermodynamic studies, J. Ind. Eng. Chem., 25 (2015) 35–41.
[37] R. Bushra, Mu. Naushad, R. Adnan, Z.A. ALOthman, M. Rafatullah, Polyaniline supported nanocomposite cation exchanger: synthesis, characterization and applications for the efficient removal of Pb^{2+} ion from aqueous medium, J. Ind. Eng. Chem., 21 (2015) 1112–1118.
[38] R. Gündoğan, B. Acemioğlu, M.H. Alma, Copper (II) adsorption from aqueous solution by herbaceous peat, J. Colloid Interface Sci., 269 (2004) 303–309.